Creep-Fatigue Crack Growth Behavior in an Ex-service Cr-Mo-V Rotor Steel

N.B. Adefris and A. Saxena
School of Materials Engineering
Georgia Institute of Technology
Atlanta, GA 30332-0245

Subcontract No. 06-1536
EPRI Research Project 2481-5
June 15, 1991.

SwRI Project Managers:
S.J. Hudak, Jr.
G. Leverant

Legal Notice

Prepared by Mechanical Properties Research Laboratory, Georgia Institute of Technology, Atlanta, GA 30332-1245, under contract with Southwest Research Institute.

Contents

List of Tables

Illustrations

Section 1
Summary and Conclusions

Creep-fatigue crack growth behavior of an ex-service Cr-Mo-V steel was investigated under hold times of 0, 0.0278, 0.25, and 8 hours for a trapezoidal loading waveform at a temperature of 538°C (1000°F). These data are compared with the creep crack growth behavior obtained on the same material by Southwest Research Institute. Non-linear finite element (FEM) analyses with various creep deformation laws as well as experiments with various hold times were performed on compact type specimens with stationary cracks. The work was aimed at developing accurate expressions for estimating $(C_t)_{avg}$ for 1Cr-1Mo-0.25V Steel at 538°C. These expressions were then used for estimating $(C_t)_{avg}$ in crack growth specimens tested under the various hold times.

When elastic-plastic-primary creep-secondary creep deformation model was used in the FEM analyses, the calculated values of C_t compared well with the measured values. The FEM results also showed that the accumulated creep during the hold time was not significantly reversed during the unloading portion of the creep-fatigue cycle. A new method of calculating $(C_t)_{avg}$, which is most suitable for this material is proposed on the basis of these numerical and experimental results.

The correlation of the crack growth rate with $(C_t)_{avg}$ was significantly improved when the new estimation scheme was used to estimate $(C_t)_{avg}$. Recommendations for additional work are also provided.

Section 2
Introduction and Background

Recently, there has been an increased interest in assessing the remaining life of highly stressed components operating at high temperatures in power plants. Dominant cracks have a tendency to develop in these components in highly stressed regions and grow under the condition of fatigue and creep in the small scale creep (SSC) regime. Therefore, characterizing creep-fatigue crack growth (CFCG) rates is an important step in predicting the design life time and the remaining life time of such components. Several CFCG models have been proposed in the past. In an early study, Saxena and co-workers [1] proposed that creep-fatigue crack growth rates in the small-scale creep regime can be correlated by a parameter related to the amplitude of the crack tip stress fields. In a later study, Saxena and Gieseke [2] proposed the use of the average value of the C_t parameter for characterizing creep-fatigue crack growth rates. C_t characterizes the Hutchinson [3], Rice and Rosengren [4] (HRR) crack tip stress field in the extensive creep regime, and is also uniquely related to the rate of expansion of the creep zone size in the small-scale creep regime. In a more recent study [5], it was shown that for some materials the effect of instantaneous plasticity on creep is considerable and it is necessary to include this effect in estimating the average value of the C_t parameter. However, plasticity-creep interactions is a material dependent phenomenon and its extent can vary from one material to another.

The objective of this report is to characterize creep-fatigue crack growth rate behavior in an ex-service rotor steel and to develop a method for estimating the magnitude of the most appropriate crack tip parameter. CFCG data were obtained by testing compact type specimens subjected to trapezoidal loading waveforms. Considerable use of nonlinear finite element analyses was made to develop accurate methods of estimating the average values of C_t.

2.1 Background

2.1.1 Constitutive Relations

A material deforming under a given state of stress, $\tilde{\sigma}$, and temperature, T, will generally obey a constitutive relation given by:

$$\dot{\tilde{\varepsilon}} = f(\tilde{\sigma}, T, t) \qquad ...(1)$$

where t is the time and $\dot{\tilde{\varepsilon}}$ is the strain rate. Generally $\dot{\tilde{\varepsilon}}$ can be partitioned into an elastic part , $\dot{\tilde{\varepsilon}}^{el}$, and a non-elastic, $\dot{\tilde{\varepsilon}}^{ne}$, part as:

$$\dot{\tilde{\varepsilon}} = \dot{\tilde{\varepsilon}}^{el} + \dot{\tilde{\varepsilon}}^{ne} \qquad ...(2)$$

The elastic strain is related to the applied stress by Hooke's law, which for a multi-axial state of stress is given by:

$$\tilde{\varepsilon}^{el} = \frac{1+\nu}{E}\tilde{\sigma} - \frac{\nu}{E}(tr(\tilde{\sigma}))\tilde{I} \qquad ...(3)$$

where ν and E are Poisson's ratio and Modulus of Elasticity respectively. The trace of the stress , $tr(\tilde{\sigma})$,is given by $\sigma_{11} + \sigma_{22} + \sigma_{33}$. For a uniaxial stress condition:

$$\tilde{\varepsilon}^{el} = \frac{\tilde{\sigma}}{E} \qquad ...(4)$$

The non-elastic component, $\dot{\tilde{\varepsilon}}^{ne}$, represents the strain rate associated with permanent (dissipative) deformation. The time-independent isotropic hardening plastic strain rate , $\dot{\tilde{\varepsilon}}^{pl}$, is given by:

$$\dot{\tilde{\varepsilon}}^{pl} = \frac{3}{2} D \dot{\tilde{\sigma}}' \left(\sqrt{\frac{3}{2}} \dot{\tilde{\sigma}}' : \dot{\tilde{\sigma}}' \right)^{(m-1)} \qquad ...(5)$$

Throughout these equations the dots, (·), represent rates, the tildes, (~), tensor quantities and the colon (:) double contraction of a tensor. D and m are material constants and $\tilde{\sigma}'$ is the deviatoric stress. For the uniaxial state of stress this relation reduces to:

$$\dot{\varepsilon}^{pl} = D\dot{\sigma}^{m} \qquad ...(6)$$

Under steady-state creep conditions, the secondary creep strain rate , $\dot{\tilde{\varepsilon}}_{(ss)}$, for multi-axial state of stress is given by:

$$\dot{\tilde{\varepsilon}}_{(ss)} = \frac{3}{2} A \tilde{\sigma}' \left(\sqrt{\frac{3}{2}} \tilde{\sigma}' : \tilde{\sigma}' \right)^{(n-1)} \qquad ...(7)$$

where A and n are material constants that depend on the temperature. For the case of uniaxial loading, Equation (7) reduces to the simple power law form:

$$\dot{\varepsilon}_{(ss)} = A\sigma^{n} \qquad ...(8)$$

For a material that shows appreciable hardening during the beginning of loading due to dislocation tangles and/or due to dislocation substructure, the non-elastic strain rate , $\dot{\tilde{\varepsilon}}_{(pc)}$, becomes a function of time as well as stress, temperature and material properties:

$$\dot{\tilde{\varepsilon}}_{(pc)} = \frac{3}{2} A_1 \tilde{\sigma}' \left(\sqrt{\frac{3}{2}} \tilde{\varepsilon}' : \tilde{\varepsilon}' \right)^{-p} \left(\sqrt{\frac{3}{2}} \tilde{\sigma}' : \tilde{\sigma}' \right)^{n_1(1+p)-1} \qquad ...(9)$$

where A_1,p and n are temperature dependent material constants and $\tilde{\varepsilon}'$ is the deviatoric strain. For the uniaxial case, Equation (9) becomes:

$$\dot{\varepsilon}_{(pc)} = A_1 \varepsilon^{-p} \sigma^{n_1(1+p)} \qquad ...(9a)$$

Thus, for a material that deforms in an 'elastic-primary creep-secondary creep', the uniaxial strain rate is given by

$$\dot{\varepsilon} = \frac{\dot{\sigma}}{E} + A\sigma^{n} + A_1 \varepsilon^{-p} \sigma^{n_1(1+p)} \qquad ...(10)$$

2.1.2 Crack Tip Parameters

a) Extensive Creep Conditions

For a cracked body under extensive steady-state creep conditions, Landes and Begley [6] proposed a path independent crack tip parameter, C*, given by:

$$C^* = \int_\Gamma W_s^* dy - \tilde{T} \cdot \left(\frac{\partial \dot{\tilde{u}}}{\partial x} \right) ds \qquad ...(11)$$

where W_s^* is the stress working power, $\dot{\tilde{u}}$ is the displacement rate vector, Γ is the contour taken from the lower crack surface to the upper crack surface in the clockwise direction, ds is a differential length along Γ, and $\tilde{T}$ is the traction vector ,a unit normal vector along Γ. C* was defined by analogy to the J-integral and represents the stress-power difference between two identical bodies under the same loading conditions with an infinitesimally differing crack lengths. For a cracked body with a thickness, B, and a crack length, *a*, C* is given by:

$$C^* = -\frac{1}{B}\frac{dU^*}{da} \qquad ...(12)$$

where U* is the power input into the cracked body. C* also represents the amplitude of the stress singularity at the crack tip under the condition of extensive secondary creep.

Under the condition of extensive primary creep, when the primary creep term in Equation (10) is said to dominate the secondary creep term, Riedel [7] has defined the C_h^* parameter to describe the amplitude of the stress singularity. C_h^* is also a path independent integral, and differs from C* by factor which depends on time. It can be shown that C* at any instant, t, is also path-independent for dominant primary creep conditions.

b) Small-Scale Creep Conditions

Under small-scale creep conditions, the strain rate is a function of time as well as stress, as described by Equation (1). The C*-integral under such circumstances will not be path independent. However, in the vicinity of the crack tip, creep strain rates dominate over elastic strain rates. If an integration path is selected in the creep dominated region, the integral given by Equation (11) will be path independent and will describe the amplitude of the crack tip stress singularity [8]. This integral, C(t), is given by:

$$C(t) = \int_{\Gamma \to 0} W^* dy - \tilde{T} \cdot \left(\frac{\partial \dot{\tilde{u}}}{\partial x} \right) ds \qquad ...(13)$$

Under the extensive creep conditions C(t) approaches C*.

Riedel and Rice [9] have derived an approximate expression for C(t) in the small scale creep (SSC) regime for a material deforming by elastic and secondary creep:

$$(C(t))_{SSC} = \frac{(1-\nu^2)K^2}{E(n+1)t} \qquad ...(14)$$

Ehlers and Riedel [10] have given an approximate interpolation scheme for calculating C(t) in between the SSC and the extensive creep regimes:

$$C(t) = (C(t))_{SSC} + C^* \qquad ...(15)$$

The transition time from the SSC to extensive creep condition, t_T, is defined by the condition $(C(t))_{SSC} = C^*$ as:

$$t_T = \frac{(1-\nu^2)K^2}{E(n+1)C^*} \qquad ...(16)$$

For a material which exhibits elastic and primary creep behavior, the transition time, t_1 , from small scale primary creep to extensive primary creep has

been defined by the condition:

$$t_1 = \frac{1}{n_1 + 1}\left[\frac{J}{C_h^*}\right]^{p+1} \qquad ...(17)$$

where J is the path-independent integral for a non-linear elastic material.

For a material that exhibits both primary and secondary creep behavior, initially the primary creep dominates the behavior, and the appropriate parameter is C_h^*. With time, a secondary creep zone evolves within the region of primary creep which eventually grows out of the primary creep zone and engulfs the entire ligament after a time, t_2, given by:

$$t_2 = \left[\frac{n+p+1}{(1+p)(n+1)}\frac{C_h^*}{C^*}\right]^{\frac{1+p}{p}} \qquad ...(18)$$

The C(t)-integral that characterizes the amplitude of the HRR field under such conditions has been given by Riedel and Detampel [11] as:

$$C(t) = (C(t)_{SSC}) + C^*\left[\left(\frac{t_2}{t}\right)^{\frac{p}{1+p}} + 1\right] \qquad ...(19)$$

One major limitation of the C(t) parameter is that it cannot be measured in the small-scale creep regime, and it lacks the experimental evidence to sufficiently support its use for characterizing the crack growth behavior in this regime.

C_t Parameter

C_t is an alternate crack tip parameter to describe small scale creep conditions. For a given cracked body with a thickness, B, and a crack of length, a, the crack tip parameter C_t was proposed by Saxena [12] as the instantaneous stress power (U_t^*) dissipation rate given by the expression:

$$C_t = \lim_{\Delta a \to 0}\left[-\frac{1}{B}\frac{\Delta U_t^*}{\Delta a}\right] = -\frac{1}{B}\frac{\partial U_t^*}{\partial a} \qquad ...(20)$$

Under the steady-state conditions of extensive secondary creep, C_t is identical to the C*-integral:

$$C_t \equiv C^* = -\frac{1}{B}\frac{dU^*}{da} \qquad ...(21)$$

The above expression is valid for any creep law of the form in which the creep rate ($\dot{\varepsilon}$) is a unique function of the stress, σ. This occurs in the steady-state region in which the steady-state creep rate can be represented, for example, by the power law relation as given by Equation (8).

Under the conditions of extensive primary creep, C_t is equal to the instantaneous value of the path independent C*-integral:

$$C_t = C^*(t) = C_h^* \frac{1}{(1+p)t^{p/(1+p)}} \qquad ...(22)$$

An expression for C_t for the small scale creep (SSC) regime is defined by applying the concept of Irwin's effective crack length:

$$a_{eff} = a + \beta r_c \qquad ...(23)$$

where β is Irwin's correction factor and a_{eff},a and r_c are the effective crack length, the actual crack length and the creep zone size, respectively [12]:

$$(C_t)_{SSC} = \frac{P(\dot{V}_c)_{SSC}}{BW}\frac{F'}{F} \qquad ...(24)$$

where P,W and $(\dot{V}_c)_{SSC}$ are applied load, specimen width, and the load line deflection rate under small-scale creep respectively. This expression allows one to conveniently measure C_t at the loading pins. F(a/W) = (KB$\sqrt{}$W)/P and F' is defined by dF/d(a/W). $(\dot{V}_c)_{SSC}$ is given by:

$$(\dot{V}_c)_{SSC} = \frac{2B(1-\nu^2)}{EP}K^2\beta\dot{r}_c(\theta,n) \qquad ...(25)$$

For components, a suitable expression for C_t in the SSC [12,13] is given by:

$$(C_t)_{SSC} = 2(1-\nu^2)\beta \frac{F'}{F} \frac{K^2 \dot{r}_c(\theta,t)}{EW} \qquad ...(26)$$

With the relationships, $r_c(\theta,t) = \alpha K^2 (EAt)^{2/(n-1)} \tilde{r}(\theta,n)$ for secondary creep and $r_c(\theta,t) \propto \alpha(n_1) K^2 (E(A_1 t)^{1/(1+p)})^{2/(n_1-1)} \tilde{r}(\theta,n_1)$ for primary creep, useful expressions have been derived by substituting the creep zone expansion rates in Equation (25).

Analogous to the definition of C(t), C_t has been defined over the entire creep range as:

$$C_t = (C_t)_{SSC} + C^* \qquad ...(27)$$

If the expression for $(C_t)_{SSC}$ from Equation (24) is substituted in the above Equation, a useful expression to measure C_t experimentally over the entire creep regime can be obtained.

$$C_t = \frac{P(\dot{V}_c - \dot{V}_{SS})}{BW} \frac{F'}{F} + C^* \qquad ...(28)$$

A wide range of expression for C_t in the presence of primary and secondary creep can be obtained by analogy to Equation (19) as:

$$C_t = (C_t)_{SSC} + C^* \left[\left(\frac{t_2}{t} \right)^{\frac{p}{1+p}} + 1 \right] \qquad ...(29)$$

The average value of C_t for creep-fatigue crack growth (CFCG) under trapezoidal loading condition is determined by averaging C_t over the hold time. This is done by integrating C_t over the hold time and dividing the integral by the hold time as given by:

$$(C_t)_{avg} = \frac{1}{t_h} \int_0^{t_h} C_t dt \qquad ...(30)$$

which for a material deforming by elastic and secondary creep will be:

$$(C_t)_{avg} = \frac{2\alpha\beta\tilde{r}_c(\theta,n)}{EW}(1-\nu^2)K^4\frac{F'}{F}(EA)^{2/(n-1)}(t_h)^{-\frac{n-1}{n-3}} + C^* \quad ...(31)$$

In a recent study [5], creep retardation due to cyclic plasticity was considered in the calculation of $(C_t)_{avg}$ by introducing a time constant, t_{pl}. It was assumed that the stress field of a material that deforms in elastic-plastic-secondary creep at time t can be represented by the stress fields of a material that deforms by elastic and secondary creep at time $t+t_{pl}$. The expression for C_t was then modified as follows:

$$C_t = \frac{4\alpha\beta\tilde{r}_c(\theta,n)}{(n-1)EW}(1-\nu^2)K^4\frac{F'}{F}(EA)^{2/(n-1)}(t+t_{pl})^{-\frac{n-1}{n-3}} + C^* \quad ...(32)$$

The effect of plasticity can then be included in the calculations of $(C_t)_{avg}$ by averaging the values of C_t given by Equation (32) between the time limits of 0 and t_h. Thus, t_{pl} is a factor that accounts for creep retardation due to cyclic plasticity.

For a material deforming by elastic, plastic and secondary creep, Equation (30) then becomes:

$$(C_t)_{avg} = \frac{2\alpha\beta\tilde{r}_c(\theta,n)}{EW}(1-\nu^2)K^4\frac{F'}{F}(EA)^{2/(n-1)}\left(\frac{(t_h+t_{pl})^{\frac{2}{n-1}} - t_{pl}^{\frac{2}{n-1}}}{t_h}\right)^{-\frac{n-1}{n-3}} + C^* \quad ...(33)$$

Section 3
Experimental Techniques and Finite Elements Analyses

3.1 Test Material and Specimen Description

The test material used in this study was from the retired Moss Landing steam turbine rotor made from 1Cr-1Mo-0.25V steel. The material had been in service for 163,000 hours at 538°C (1000°F) . The chemical composition of this material is given in Table 1. The creep-fatigue crack growth tests were conducted using the standard 1T Compact Type (CT) specimens shown in Figure 1. Some specimens tested were 0.5 inch thick but had the same in-plane dimensions as a standard 1T specimen. A schematic of these specimens is also shown in Figure 1. The CT specimens were taken from the bore as well as the rim regions of the rotor. The locations of the various specimens tested are shown in Table 2.

3.2 Creep Deformation testing

The creep deformation data for this material were obtained from Southwest Research Institute (SwRI) [14]. However, these data were at high stress values in the range of 172-207 MPa (25-30 ksi). To supplement these data, a creep deformation test at a stress of 207 MPa (30 ksi) was performed according to ASTM E139-79 [15].

3.3 Creep-Fatigue Testing

3.3.1 Stationary Crack Calibration Tests

Two tests, one with a 0.0278 hour hold time and another with a 0.25 hour hold time were specially performed in order to measure the load-line deflection as a function of time during the hold period. The measured values of C_t were obtained

from these experiments. The load-line deflection was measured using a high temperature capacitance clip gage. The specimens were precracked under fast fatigue loading to a specific crack length and then the desired hold time was applied at a predetermined load. The load-line deflection during the hold time was measured for several fatigue cycles which was subsequently used to estimate $(C_t)_{avg}$. These values of $(C_t)_{avg}$ were then compared to analytically estimated values of $(C_t)_{avg}$ and those obtained from finite element analyses. Thus, a suitable expression for estimating $(C_t)_{avg}$ was developed for reducing the data obtained from the creep-fatigue crack growth tests.

3.3.2 Creep-Fatigue Crack Growth Tests

Creep fatigue crack growth tests were conducted on four specimens without side grooves. The remaining specimens were side grooved ten percent on each side to assure a straight crack front. The initial values of ΔK, ranged from 22 MPa$\sqrt{m}$ to 40 MPa$\sqrt{m}$. The complete matrix of tests that were performed is given in Table 2.

The experiments with hold times of 100 seconds or more were conducted using a dead weight, lever arm type creep frame with a provision to cycle the applied load using a pneumatic ram controlled by an OMEGA 2260 controller. Load on the specimen was directly monitored using a load cell in the load-train. The creep machines were equipped with a resistance furnace to heat the specimen. Some tests were performed in a high purity nitrogen environment in a specially designed chamber. Crack growth rates were monitored using the DC electric potential method [16]. In some tests the load line deflection was monitored using a high temperature capacitance clip gage. All the creep-fatigue specimens were fatigue precracked in accordance with ASTM E399 using a servo-hydraulic test system under load control condition at room temperature. After fatigue precracking, the specimens were subjected to trapezoidal load cycle with hold times of 0.0278 hour, 0.25 hour and 8 hours, respectively at 538^{o}C (1000^{o}F). The loading and unloading durations were six seconds each. Experiments with a triangular loading waveform at frequencies of 0.5 Hz and 0.083 Hz were also performed without hold time to

assess the contributions of the loading and unloading portions of a cycle to the overall creep-fatigue crack propagation rate.

3.4 Finite Element Analyses

Finite element analyses was carried out using the code originally developed by Hinton and Owen [17] and modified by McDowell and Leung [18,19] to include a kinematic hardening plasticity model.

3.4.1 Description of the Model

Detailed description of the model regarding the computational procedures and the code structure as well as program listing can be found in the literature [17]. At this point, only brief discussion of the analyses is appropriate. McDowell and Leung [18,19] have modified the original program which included Elastic, Isotropic hardening plasticity, Classical strain hardening primary creep and Power law creep. The modification that was applied to the original code was the inclusion of rate independent state variable plasticity model instead of an isotropic hardening plasticity. This will apply for the non-linear kinematic hardening associated with cyclic loading. Like the original version, the total strain increment was also partitioned into elastic, plastic and creep component in this model. Evaluation of the creep increment, $\dot{\tilde{\varepsilon}}_p$, was given by:

$$\dot{\tilde{\varepsilon}}_p = \frac{1}{h}\left\langle \dot{\tilde{\sigma}}' : \tilde{n} \right\rangle \qquad \ldots(34)$$

where $\dot{\tilde{\sigma}}'$ is the deviatoric stress rate and the unit normal, $\tilde{n}$,is given by:

$$\tilde{n} = \frac{\tilde{\sigma} - \tilde{\alpha}}{\left\| \tilde{\sigma} - \tilde{\alpha} \right\|} \qquad \ldots(35)$$

The Macauley bracket,< > , in Equation (9) is defined as the argument if the argument within the bracket is positive and it becomes zero when the argument is

negative (or zero). The sign $\|\tilde{\sigma}-\tilde{\alpha}\|=\left[(\tilde{\sigma}-\tilde{\alpha}):(\tilde{\sigma}-\tilde{\alpha})\right]^{1/2}$. The hardening modulus, h, is given by:

$$h = H^*(b^*\tilde{n}-\tilde{\alpha}^*):\tilde{n}+C(\delta)(b\tilde{n}-\tilde{\alpha}^s):\tilde{n} \qquad ...(36)$$

$$\delta = \|b\tilde{n}-\tilde{\alpha}^s\| \qquad ...(37)$$

$$\dot{\tilde{\alpha}} = \dot{\tilde{\alpha}}^s + \dot{\tilde{\alpha}}^* \qquad ...(38)$$

where $\tilde{\alpha}$ is the deviatoric back stress and $\tilde{\alpha}^*$ and $\tilde{\alpha}^s$ are the long range and the short range deviatoric back stresses, respectively. b* and b are the amplitude of the long range and short range internal stresses respectively.

The yield and bounding surfaces are given by the von-Misses form as:

$$f = (3/2)^{1/2}\|\tilde{\sigma}'-\tilde{\alpha}\|-R^2 \qquad ...(39)$$

$$f^* = (3/2)^{1/2}\|\tilde{\sigma}'-\tilde{\alpha}^*\|-R^{*2} \qquad ...(40)$$

where R and R* are the yield and bounding surface radii respectively.

$$C(\delta) = k_1 + k_2\left[\sinh\left(k_3\frac{\delta}{2b}\right)\right]^{k_4} \qquad ...(41)$$

k_1, k_2, k_3, k_4, H^*, and $C(\delta)$ are hardening related constants. Through out these equations the dots, (·), represented rates and the tildes, (~), tensor quantities. Since cyclically stable stress and strain conditions are examined, the present formulation employs only kinematic hardening.Thus:

$$\dot{R} = \dot{b} = 0$$

During each time increment, the field and state variables were updated by using central difference approximation. Convergence was determined by calculating the residual forces and adding them to the applied force increment in the next time step.

In order to gain numerical stability, the implicit trapezoidal marching scheme was employed. The maximum effective creep strain increment did not exceed 15% of the total load increment in order to increase the accuracy. The current time step increments were not more than 150% of the previous time step increment to avoid oscillatory solution. Further details of the finite element code is found in references [17,18,19].

3.4.2 Cases Analyzed by FEM

Data on the monotonic stress-strain behavior in this material was obtained from SwRI [14]. The material was assumed to be cyclically stable and the cyclic stress-strain behavior was approximated by the monotonic stress-strain curve. Since this material has been shown to exhibit some cyclic softening [20,21,22], this assumption is approximate. The necessary plasticity constants for the FEM were obtained by fitting the monotonic stress-strain curve. The list of the constants used is presented in Table 3.

Plane strain analyses of a specimen with a thickness of 25.4 mm (1 in) and a width of 50.8 mm (2 in) was performed using a finite element mesh of 202 isoparametric elements with straight edges. At the crack tip, degenerated elements were created by collapsing 3 nodes along one side into one initial point, at the same time allowing them to deform independently. These degenerated elements produced a $1/r$ type singularity in displacement derivatives leading to the achievement of an acceptable approximation of $r^{-n/(1-n)}$ HRR singularity. A crack length, a, of 20.38 mm (0.8 in) giving a crack ratio (a/W) of 0.4 was investigated. The applied load was distributed over the upper portion of the pin hole over a span of 45^0.

Section 4
Results and Discussion

4.1 Creep deformation

Steady-state creep strain rate as a function of the applied stress is shown in Figure 2. The data on this figure include previous data on Cr-Mo-V steel from the literature [23] as well as the data from SwRI tests conducted on the Moss Landing rotor material. The results obtained in this study at a stress level of 207 MPa (30 ksi) are also included. The previous data exhibited better fit when the strain rate is related to the applied stress by using a power-law relationship containing two terms:

$$\dot{\varepsilon}_{(ss)} = A'\sigma^{n'} + A''\sigma^{n''} \qquad ...(42)$$

The values of A',A'' ,n' and n'' were found to be 1.49×10^{-16}(ksi)$^{-7}$/hr, 9.65×10^{-35} (ksi)$^{-13}$/hr,7 and 13, respectively. Another approach for representing the creep data is to use the hyperbolic sine function as proposed by Bassani [24]. The advantage of using a power-law relation is that the analytical expressions for estimating crack tip parameters are readily available for such constitutive relations and are not available for the hyperbolic sine model. In this study, a single value of 8 for the exponent, n, and 1.24×10^{-24} (MPa)$^{-8}$/hr for A were used. The fit obtained by employing these values of A and n is also shown in Figure 2. This material also showed evidence of primary creep deformation. Primary creep data were obtained from SwRI tests as well as from the literature data and primary creep constants were derived by fitting Equation (9a) to the data. All the creep deformation constants are presented in Table 4.

4.2 Verification of the Methods for Estimating C_t and $(C_t)_{avg}$

In order to select a proper constitutive model for the creep deformation in the FEM, measured values of C_t were obtained during a hold time of 0.0278 hour and 0.25 hour. C_t values were determined from Equation (24) using the values of

measured load-line deflection rates. These values are presented in Figure 3 as a function of time normalized with respect to the transition time of a 1T CT specimen with a crack to width ratio, a/W, of 0.4 and loaded to a stress intensity factor, ΔK, of 22 MPa$\sqrt{m}$ (20 ksi$\sqrt{in}$). Figure 3 also shows the results the first cycle of a 0.0278 hour hold time FEM results predicted from elastic-secondary creep model. Since the results from the static FEM analyses agree entirely with the results from the analytical estimation for an elastic-secondary creep model, the accuracy of the finite element code is verified. Due to the considerable discrepancy between the analytical (or FEM) results and the measured values of C_t, it is concluded that the elastic-secondary creep model is not adequate for representing the creep behavior of the Moss Landing material. Figure 4 shows the FEM results for a similar situation predicted for a material deforming by elastic, plastic and secondary creep. During the hold time for a material that obeys such a constitutive relation, C_t appears to be relatively independent of time. The values of C_t obtained using this model are considerably lower than the ones that were experimentally measured during the hold time. Also shown in Figure 4 are analytically predicted values of C_t for the first cycle for an elastic-plastic secondary creep material. In order to fit the FEM results, a t_{pl} value of 0.3 hour was used in equation (33). The prediction from this model deviates from the experimental data even more than the prediction from an elastic, secondary-creep model. Hence, this representation is also indequate.

Figure 5a shows FEM prediction for elastic-plastic-primary and secondary creep model. In this figure three cycles of 20 minutes hold time are presented and the time at the beginning of each cycle was set to zero. The values of C_t appear to be slightly lower than the experimentally observed values during the first 100 seconds of the first cycle. At higher times these differences disappeared. The introduction of primary creep also appears to reduce the t_{pl} value significantly. t_{pl} reduces to 0.004 hrs for primary creep from a value of 0.3 hrs without primary creep.

Another method of representing the data in Figure 5a is to let the time at the end of the previous cycle be the time at the beginning of the current cycle as shown in Figure 5b. It appears from these figure that the C_t values obtained from the FEM

for the three cycles are not significantly affected by the unloading and reloading. In other words, the magnitude of C_t at the beginning of the hold period during any cycle is approximately equal to the C_t value at the end of the previous cycle. It appears that the creep deformation is not significantly reversed by plastic deformation during unloading. The experimental values of C_t during the 15 minutes hold time also appear to agree with the FEM values of C_t for the three cycles when time is considered cumulatively. This is further evidence that the C_t values for 0.0278 hrs hold time are not significantly affected by the unloading-reloading. Thus, when the specimen is loaded again the creep deformation process resumes with no significant influence from the load cycling. There was also a significant difference in the values of C_t between the second and the third cycle in the FEM analyses. These observations are significantly different from the observations of Yoon *et. al.* [5] from a similar analyses on 1.25Cr-0.5Mo steels.

Figure 6 shows the relative sizes of the monotonic plastic zone, cyclic plastic zone and creep zone at the end of the third cycle for a hold time of 20 minutes. The monotonic plastic zone boundary is defined by the locus of points where $\bar{\varepsilon}_p/\bar{\varepsilon}_e = 1$,the creep zone boundary by the locus of points where $\bar{\varepsilon}_c/\bar{\varepsilon}_e = 1$, and the cyclic plastic zone boundary is defined by the locus of points where $\Delta\bar{\varepsilon}_{pl}/\Delta\bar{\varepsilon}_{el} = 1$ where $\bar{\varepsilon}_e, \bar{\varepsilon}_p$ and $\bar{\varepsilon}_c$ are effective elastic, plastic and creep strains respectively. Δ represents the differences in strains between the end of a hold time and the beginning of the next cycle. The cyclic plastic zone was found to be inside the creep zone in Figure 6 suggesting the domination of creep over fatigue in this material. Similar plots for 1.25Cr-0.5Mo Steels [5] have shown that the cyclic plastic zone entirely engulfed the creep zone at the end of the third cycle of a 600 sec. hold time FEM simulation. It should be pointed out that the plastic and the creep zones constructed in the above figures are derived from very few gauss points. The mesh sizes of 0.127 mm (0.005 in) were comparable to the creep and plastic zone sizes, which may explain the distorted plastic and creep zone shapes in Figure 6.

4.3 Suggested Modifications for the method of Estimating $(C_t)_{avg}$ in Cr-Mo-V Steel

In the previous section, it was shown that the effect of loading and unloading during creep-fatigue crack growth on the stress-strain behavior in this material is not considerable. It was also shown that the values of C_t beyond the first cycle did not deviate appreciably from the monotonic values of C_t. This leads to the conclusion that for subsequent cycles, resetting the value of C_t to its value at the beginning of the initial hold time as given by Equation (30) may not be proper in this material. In this section a new approximation method for estimating $(C_t)_{avg}$ for this material is presented.

It is proposed that reversal of the accumulated creep deformation during the hold time by a single fatigue cycle (unloading and reloading) may not be possible in 1Cr-1Mo-0.25V steels. This is due to the high cyclic yield strength of this material as compared to 1.25Cr-0.5Mo steels [5]. The high cyclic yield strength leads to a small cyclic plastic zone which is surpassed in size by the creep zone for relatively small hold times. In order to reverse the creep accumulated during the hold time, it may be necessary to provide a hold time at the minimum load.

If it is assumed that the creep deformation which is reversed by cyclic plasticity is negligible, a modification to the approach for estimating $(C_t)_{avg}$ is necessary. The analytical expression for C_t in small scale creep (SSC) regime has been given as [13]:

$$(C_t)_{SSC} = \frac{4\alpha\beta\tilde{r}_c(\theta,n)}{EW(n-1)}(1-\nu^2)K^4\frac{F'}{F}(EA)^{2/(n-1)}t^{-\frac{n-1}{n-3}} \quad ...(43)$$

$$\alpha = \frac{1}{2\pi}\left[\frac{(n+1)I_n}{2\pi(1-\nu^2)}\right]^{\frac{2}{n-1}}$$

where I_n is a dimensionless parameter related to the HRR stress field [25].

The average value of C_t for creep-fatigue crack growth (CFCG) is determined by averaging C_t over the hold time, as given by equations (30) and (31).

For an arbitrary N^{th} cycle the value of $(C_t)_{avg}$ can be given as follows:

$$(C_t)_{avg} = \frac{1}{t_h}\int_{(N-1)t_h}^{Nt_h} C_t dt \qquad ...(44)$$

which, upon integration will give:

$$(C_t)_{avg} = \frac{2\alpha\beta\tilde{r}_c(\theta,n)}{EW}(1-\nu^2)K^4\frac{F'}{F}(EA)^{2/(n-1)}\left[N^{2/n-1}-(N-1)^{2/n-1}\right](t_h)^{-\frac{n-1}{n-3}}+C^* \qquad ...(45)$$

This expression makes $(C_t)_{avg}$ not only a function of crack length and applied stress but also of time because of the term related to the number of cycles, N. This equation can further be simplified as follows if the value $(N-1)^{2/n-1}$ could be approximated using binomial expansion:

$$C_t = \frac{4\alpha\beta\tilde{r}_c(\theta,n)}{(n-1)EW}(1-\nu^2)K^4\frac{F'}{F}(EA)^{2/(n-1)}(Nt_h)^{-\frac{n-1}{n-3}}+C^* \qquad ...(46)$$

This representation is identical to the analytical C_t expression proposed by Bassani *et al* [13], with the value Nt_h replacing time.

Using a similar method for elastic-primary creep-secondary creep material the following approximate expression for $(C_t)_{avg}$ can be derived from Equation (29):

$$(C_t)_{avg} = \left((C_t)_{SSC}\right)^{t=Nt_h} + C^*\left[\left(\frac{t_2}{Nt_h}\right)^{\frac{p}{1+p}}+1\right] \qquad ...(47)$$

$(C_t)_{SSC}$ for elastic-primary creep-secondary creep material is given by :

$$(C_t)_{SSC} = \frac{2\beta\tilde{r}_c(\theta,n_1)}{\pi EW}\frac{(1-\nu^2)K^4}{(1+p)(n_1-1)}\frac{F'}{F}((n_1+1)(1+p)A_1)^{2/(1+p)(n_1-1)}\left[\frac{I_{n_1}E}{2\pi(1-\nu^2)}\right]^{\frac{2}{n_1-1}} t^{\left[\frac{2}{(n_1+1)(1+p)}-1\right]} \qquad ...(48)$$

where I_{n_1} is a dimensionless factor related to the HRR field.[25]

4.4 Creep-Fatigue Crack Growth Test Results

Creep-fatigue crack growth (CFCG) data for Cr-Mo-V turbine rotor steel have been reported previously [26,27]. Plots of stress intensity factor, ΔK, versus cyclic crack growth rates, da/dN, have been used in the past to represent CFCG behavior. Recently, CFCG data has been correlated with the $(C_t)_{avg}$ parameter [2,5,28] in which the average value of da/dt during hold time is correlated with the average value of C_t during the hold time. Both types of data representations are given in this report.

4.4.1 da/dN versus ΔK Behavior

Figure 7 shows the cyclic crack growth rate, da/dN, as a function of the stress intensity factor, ΔK, for hold times of 0.0278 hour, 0.25 hour and 8 hours respectively. The results from the 1 Hz and 0.083 Hz tests with no hold times are also included on this Figure. The crack growth rates generally increase with increasing hold times. For the tests conducted with 0.0278 hour hold time the crack growth rate at the low ΔK values exhibited lower crack growth rates than the tests conducted at 1 Hz with no hold times. The same effect was also observed when comparing the 0.0278 hour hold time with the 0.083 Hz data with no hold time. A possible explanation could be due to crack tip blunting which occurs during the hold time and possibly reduces the stresses around the crack tip as compared to a sharp fatigue crack.

Figure 8 shows the effect of specimen location within the rotor (Bore versus Rim) on the cyclic crack growth rate. The rim material appears to have a slightly higher crack growth rate at a given ΔK in comparison to the bore material at a cyclic frequency of 1 Hz without hold time. The effect is even less significant when the hold time is 0.0278 hours. Therefore, for the purposes of creep-fatigue crack growth behavior, no distinction will be made between the properties of the bore and the rim regions of the rotor material.

4.4.2 da/dt versus $(C_t)_{avg}$ Behavior

The total crack growth rate was partitioned into a cycle dependent part and a time-dependent part (as in [1,2,5,28]):

$$\frac{da}{dN} = \left(\frac{da}{dN}\right)_{cycle} + \left(\frac{da}{dN}\right)_{time} \qquad ...(49)$$

And the crack growth rate during the hold time is given by:

$$\left(\frac{da}{dt}\right)_{avg} = \frac{1}{t_h}\left[\frac{da}{dN} - \left(\frac{da}{dN}\right)_{cycle}\right] \qquad ...(50)$$

Paris' fatigue crack propagation law was used to represent the cyclic-part of the crack growth rate. Paris-law coefficient and exponents were determined from the 0.083 Hz data shown in Figure (7) as 2.28×10^{-18} in(ksi$\sqrt{\text{in}}$)$^{-2.2}$ and 2.2 respectively. In this study da/dt refers to the average value of crack growth rate during the hold time as defined Equation (50).

Figure 9 shows the representation of the creep-fatigue crack growth rate data as a function of $(C_t)_{avg}$ as defined by Equations (46) for a material deforming by elastic and secondary creep. For a given $(C_t)_{avg}$, the values of crack growth rate seem to be much higher in CFCG than in CCG. This may be partly due to the under-estimation of $(C_t)_{avg}$ when only secondary creep deformation is considered as was also observed in the finite element analyses results. Crack growth rate data as a function of $(C_t)_{avg}$ as defined by Equations (44) for a material deforming by elastic, primary creep and secondary creep is shown in Figure 10. This representation collapses all the creep fatigue crack growth data as well as the creep crack growth data from SwRI into a single trend with a significantly less scatter. The CFCG data are presented again in Figure 11 along with the scatter band for the creep crack growth data for the same material as well as the scatter band for a new Cr-Mo-V steel data obtained from the literature [23]. Creep fatigue crack growth in this ex-service material is significantly higher than in the new Cr-Mo-V material.

4.4.3 Effect of the Environment

CFCG tests in high purity Nitrogen environment were conducted with a 0.0278 hour hold time. The results are presented in Figures 12 as correlations of da/dN versus ΔK. The crack growth rates in this environment seem to be comparable to the tests in air. However, upon correlating the same data with $(C_t)_{avg}$ values obtained by Equation (47) the crack growth rates for a given $(C_t)_{avg}$ were found to be higher in air than in nitrogen environment as shown in Figure 13. This could be due to oxide induced cracking as reported in Cr-Mo-V steels during high cycle fatigue in the past [29]. A CFCG test in vacuum environment should be done to further understand the effect of environment.

Section 5
Recommendations for Future Work

The scheme for estimating $(C_t)_{avg}$ represented by Equation (44) is an extreme case where little creep deformation is reversed by cyclic plasticity. An experiment should be performed on the same material with a balanced loading waveform (with hold times both at the maximum and minimum loads). This will provide additional insight into the extent to which creep can be reversed under these conditions. Other areas that need more work are:

i. The influence of cyclic hardening and softening on the reversal of the accumulated creep deformation during hold time by cyclic plasticity should be analytically explored. This will lead to expressions for estimating $(C_t)_{avg}$ for conditions ranging from complete reversal of creep, which appears to be the case for 1.25Cr-0.5Mo steel, to the case of very little creep reversal as demonstrated by 1Cr-1Mo-0.25V steel.

ii. The effect of the environment is still not well understood in this material. More work is needed in inert and vacuum environments to determine the effects of oxide induced cracking and oxide induced crack closure.

iii. The effect of loading rate and waveform is still not well understood in this material and more work needs to be done to study creep-fatigue crack growth during slow loading and unloading. Such an effect can be seen in Figure [7] where due to some contribution of creep the crack growth rates in the 0.083 Hz test are higher than the crack growth rates in the 0.5 Hz test.

References

1. Saxena,A., R.S.Williams and T.T. Shih, " A Model for Representing and Predicting the Influence of Hold Time on Fatigue Crack Growth Behavior at Elevated Temperature", *Fracture Mechanics Thirteenth Conference*, ASTM STP 743, American Society for Testing Materials, 1981, pp 86-99.

2. Saxena, A. and B.Gieseke,"Transients in Elevated Temperatures Crack Growth", Seminar Proceedings of MECAMAT, International Seminar on High Temperature Fracture Mechanisms and Mechanics, Dourdan, France, 1987, Vol. III,pp 19-36.

3. Hutchinson, J.W., "Singular Behavior at the End of a Tensile Crack in a Hardening Material", *Journal of Mechanics and Physics of solids*, Vol. 16, 1968 , pp 13-31.

4. Rice,J.R. and G.F.Rosengren, Plane Strain Deformation Near a Crack Tip in a Power Law Hardening Material", *Journal of Mechanics and Physics of solids*, Vol. 16, 1968, pp 1-12.

5. Yoon, K., A. Saxena and D.L. McDowell, "Influence of Crack Tip Cyclic Plastic on Creep Fatigue Crack Growth", *22nd ASTM National Symposium on Fracture Mechanics*, June 1990. (to appear in the related STP - in press)

6. Landes, J.D., and J.A. Begley, "A Fracture Mechanics Approach to Creep Crack Growth", *Cracks and Fracture*, ASTM STP 590, American Society for Testing Materials, 1976, pp 128-148.

7. Riedel,H., "Creep Deformation at Crack Tips in Elastic Visco-Plastic Solids", *Journal of Mechanics and Physics of Solids*, Vol.29, 1981, pp 35-44.

8. Bassani, J.L. and F.A. McClintock,"Creep Relaxation of Stress Around a Crack Tip", *International Journal of Solids and Structures*, 7,1981, pp. 479-492.

9. Riedel, H. and J. Rice,"Tensile Cracks in Creeping Solids", *Fracture Mechanics Twelfth Conference*, ASTM STP 700, American Society for Testing Materials, 1980, pp 112-130.

10. Ehlers, R. and H. Riedel, " A Finite Element Analyses of Creep Deformation in a Specimen Containing a macroscopic crack", *Advances in Fracture Research: Proceedings of the Fifth International Conference in Fracture*, ICF-5,Vol.2, Pergamon Press, 1981, pp 691-698.

11. Riedel, H. and V. Detampel, "Creep Crack Growth in Ductile, Creep Resistant Steels", *International Journal of Fracture*, 33, 1987, pp 239-262.

12. Saxena, A., " Creep Crack Growth under Non-steady state conditions", *17th ASTM National Symposium on Fracture Mechanics, ASTM special Technical Publication*, STP 905, 1986, pp 185-201.

13. Bassani,J.L., D.E. Hawk and A. Saxena, "Evaluation of the C_t Parameter for the Characterization Creep Crack Growth Rate in the Transient Regime", *Nonlinear Fracture Mechanics: Time Dependent Fracture*, A. Saxena, J.D. Landes and J.L. Bassani, Eds., American Society for Testing Materials, Vol. I, 1989, pp.7-29.

14. Bartlett, M.L., unpublished data, South West Research Institute(SwRI), San Antonio, TX, 1990.

15. *ASTM Standards*, Part 10, Vol.10, American Society for Testing Materials, 1982, pp 332.

16. Schwalbe, K.H., and D. Helman, " Application of the Electric Potential Method to Crack Length Measurement Using Johnson's Formula", *Journal of Testing and Evaluation*, 9(3), 1981,pp 218-221.

17. Owen D.R.J., and E. Hinton, *Finite Elements in Plasticity*, Pineridge Press Limited, 1980.

18. McDowell D.L., and C.P. Leung, "Estimation of the C_t Parameter for Primary Creep", *Technical Report*, GA technologies, Palo Alto, CA, 1988.

19. Leung C.P.,"Estimation of the C_t Parameter for Primary Creep", *PhD Thesis*, George W Woodruff School of Mechanical Engineering, Georgia Institute of Technology, 1988.

20. Knazawa K., K.J. Miller and M.W. Brown, "Cyclic Deformation of 1%Cr-Mo-V Steel under Out of Phase Loads", *Fatigue of Engineering Materials and Structures*, Vol. 2, 1979, pp 217-228.

21. Brown M.W. and K.J. Miller, "Biaxial Cyclic Deformation Behavior of Steels", *Fatigue in Engineering Materials and Structures*, Vol. 1, 1979, pp 93-106.

22. Bhambri, S.K., C.R.Prasad and R.Vasuduvan, "Low Cycle Fatigue Behavior of 1Cr-Mo-V steel with Bainite and Ferrite Micro-structure", *International Journal of Fatigue*, Vol. 9, No 3, 1987, pp 239-246.

23. Saxena, A. and J. Han, "Evaluation of Crack Tip Parameters for Characterizing Crack Growth Behavior in Creeping Material", *ASTM Task Group Report* , FFRL, Georgia Institute of Technology, 1986.

24. Bassani, J.L.,"Cracks in Material with Hyperbolic Sine Law",Elastic - Plastic Fracture: Second Symposium, *Vol.I-Inelastic Crack Analyses*, ASTM STP 803, C.F. Shih, and J.P. Gudas, Eds.,American Society for Testing Materials, 1983, pp I/532-I/550.

25. Shih, C.F., *Table of Huchinson-Rice-Rosengren Singular Field Quantities"*, Technical Report MRL E-147, Brown University, Providence, RI, June 1983.

26. Saxena A. and J.L.Bassani," Time Dependent Fatigue Crack Growth Behavior at Elevated Temperatures", *Fracture: Interactions of Microstructure Mechanisms and Mechanics*, TMS-AIME, Warrendel, PA, 1984, pp 357-383.

27. James, L.A.," The Effect of Frequency upon Fatigue Crack Growth of Type 304 Stainless Steel at 1000 F", *Stress Analyses and Growth of Cracks*, Part I, ASTM STP 513,American Society for Testing Materials, 1972, pp 218-229.

28. Banerji, K. and A. Saxena, "Creep Fatigue Crack Growth in Steam Turbine Rotor Steels ", *Electric Power Research Institute Project*, RP2481-5,1987.

29. Haigh, J.R. and R.P.Skelton, " Oxidation Assisted Crack Growth during High Cycle Fatigue of 1%Cr-Mo-V at 550^{O}C", *Materials Science and Engineering*, 26, 1988, pp 524-529.

Data Source	ASTM	Moss Landing
C	0.31	0.35
Cr	1.13	1.05
Mo	1.15	1.29
Mn	0.78	0.8
V	0.23	0.27
Ni	0.33	0.16
Si	0.23	0.27
P	0.007	0.035
S	<0.001	0.03
Al	0.004	<0.01
Sn		0.01
Sb	0.0012	<0.01
As	0.003	
Cu	0.004	0.09

Table 1: Elemental Composition (%wt) of New and Moss Landing Rotor Steel

Specimen	Hold Time	Loading Time	Nominal Thickness	Net Thickness	Initial Crack Length	Final Crack Length	Maximum Load
	hrs	sec	mm(in)	mm(in)	mm(in)	mm(in)	kN(kips)
MLCT10/Bore	0	1	25.4(1)	25.4(1)	22.9(0.901)	34.8(1.370)	16.67(3.74)
MLCT12/Bore	0	1	25.4(1)	25.4(1)	24.0(0.946)	35.7(1.407)	15.50(3.7)
MLRCT09/Rim	0	1	25.4(1)	25.4(1)	23.0(0.907)	36.8(1.448)	14.72(3.3)
MLCT13/Bore	0	6	25.4(1)	25.4(1)	23.1(0.909)	34.0(1.339)	16.50(3.7)
MLCT11/Bore	0.0278	6	25.4(1)	25.4(1)	25.8(1.018)	37.3(1.467)	18.28(4.1)
MLRCT08/Rim	0.0278	6	25.4(1)	25.4(1)	26.1(1.028)	37.1(1.463)	16.50(3.7)
MLRCT10/Rim	0.0278	6	25.4(1)	25.4(1)	23.6(0.931)	36.5(1.437)	18.28(4.1)
MLCT14/Bore*	0.0278	6	25.4(1)	20.6(0.81)	23.0(0.906)	29.5(1.171)	17.39(3.9)
MLCT15/Bore	0.25	6	25.4(1)	20.3(0.8)	24.2(0.953)	42.1(1.656	17.39(3.9)
MLCTG3/Bore	0.25	6	12.7(0.5)	10.2(0.4)	15.2(0.600)	35.2(1.389)	15.83(3.55)
MLCTM1/Bore	8	6	12.7(0.5)	10.2(0.4)	15.4(0.605)	27.6(1.087)	13.38(3.0)
MLCTM2/Bore	8	6	12.7(0.5)	10.2(0.4)	17.5(0.690)	21.0(0.826)	17.84(4.0)
MLCTN1/Bore §	0.0278	6	12.7(0.5)	10.2(0.4)			
MLCTN2/Bore §	0.25	6	12.7(0.5)	10.2(0.4)			

* Test conducted in Nitrogen environment § Tests for measuring Load line Deflection

Table 2: Description of the Tests Conducted in the Study of CFCG

Variable		Units
b	208.3(30.21)	MPa(ksi)
b*	2758(400)	MPa(ksi)
k1	800	
k2	12000	
k3	1.5	
k4	2.5	
H*	3.45(0.5)	
R	240(35)	MPa(ksi)

Table 3 : Rate Independent State Variable Plasticity Constants at 538 C (1000 F)

Elastic Properties at 538 C (1000 F)

E	162 GPa (23500ksi)
n	0.3
Yield Stress	473 MPa (68.44ksi)

Plasicity Constants (Ramberg-Osgood) at 538 C(1000 F)

	-m MPa	-m ksi
D	9.5E-61	1.23E-42
m	21.6	21.6

Secondary Creep Constants

	-n MPa /hr	-n ksi /hr
A	1.14E-24	5.95E-18
n	8	8

Primary Creep Constants

	-n1(1+p) MPa /hr	-n1(1+p) ksi /hr
A1	6.17E-25	4.516E-20
p	1.99	1.99
n1	1.94	1.94

Table 4: Elastic,Plastic,Primary Creep and Secondary Creep Constants for Cr-Mo-V rotor Steel

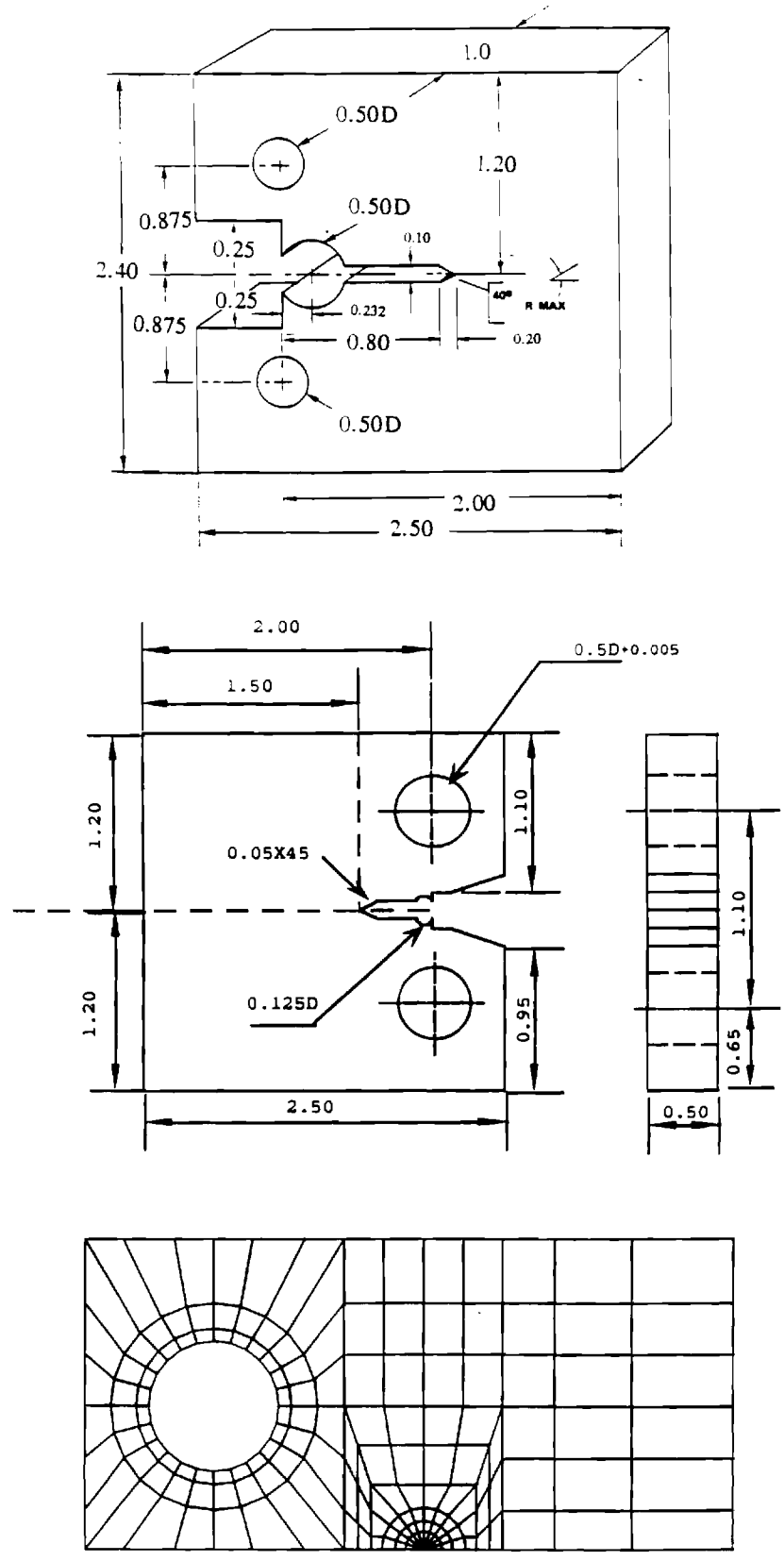

Figure 1: Compact type (CT) creep-fatigue crack growth specimen geometry and the finite element mesh used in the computational studies. (all dimensions in inches, 1 inch= 25.4 mm)

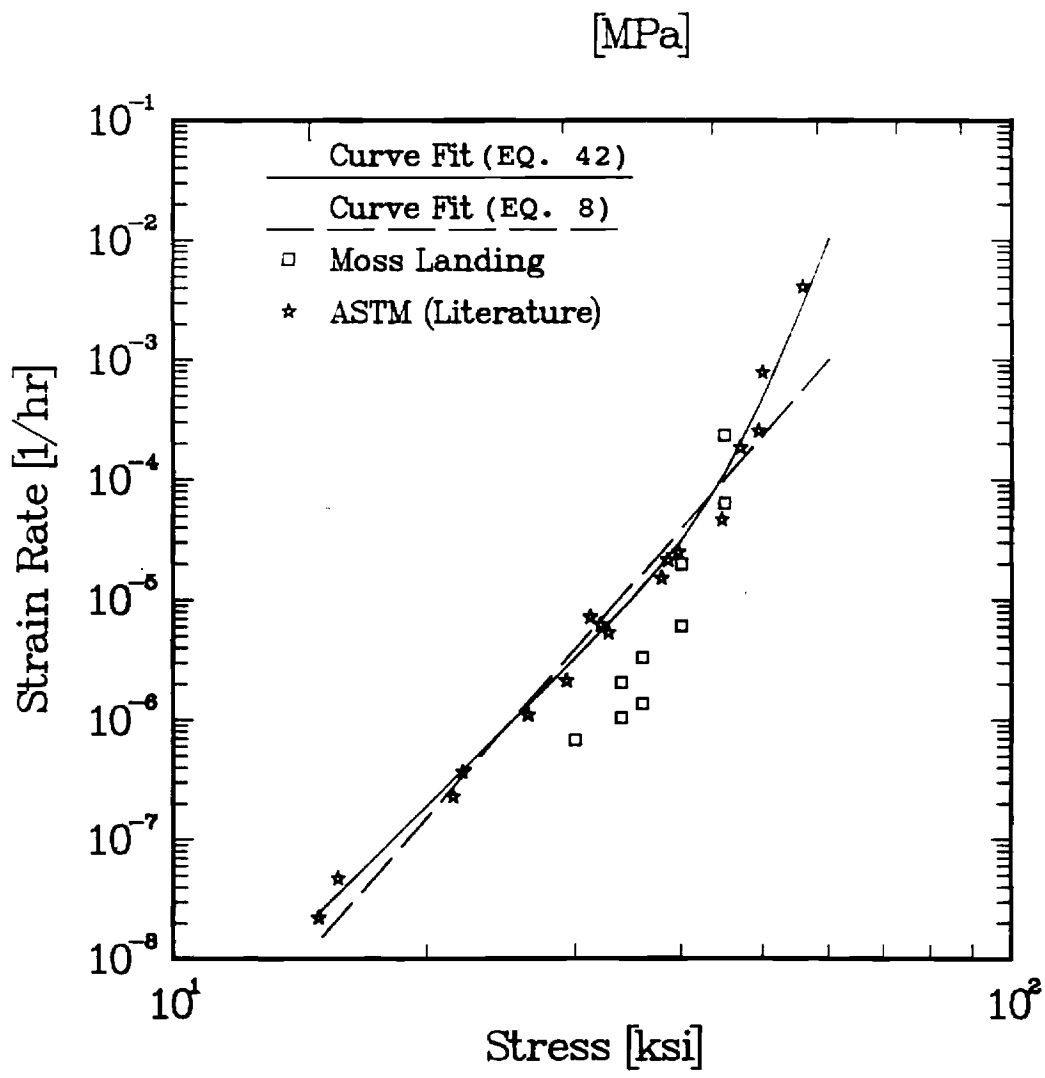

Figure 2: Steady-state creep strain rate as a function of the applied stress.

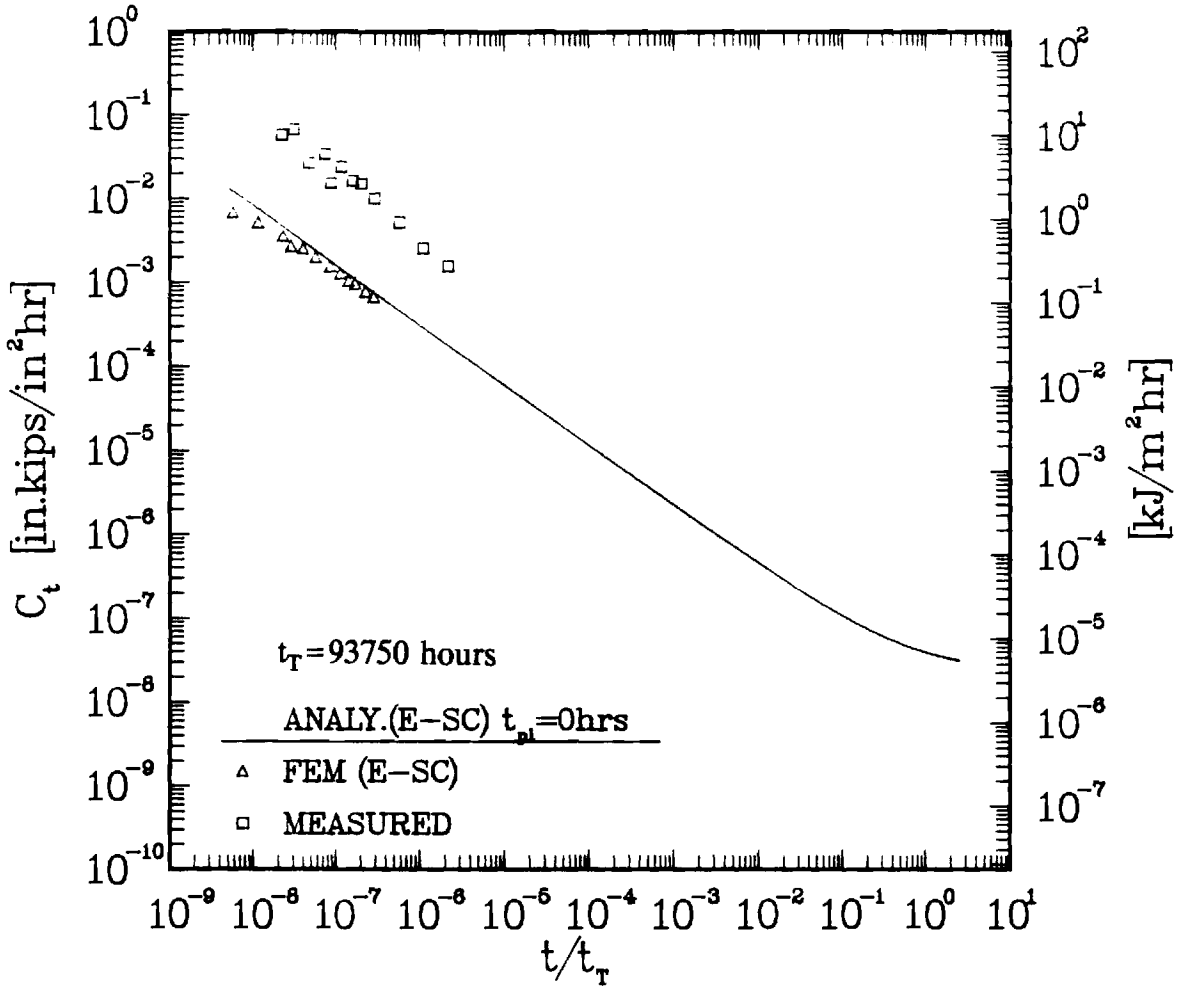

Figure 3: Measured C_t values from the first cycle of a 0.0278 hour hold time test compared with FEM and analytical prediction for an elastic-secondary creep model.

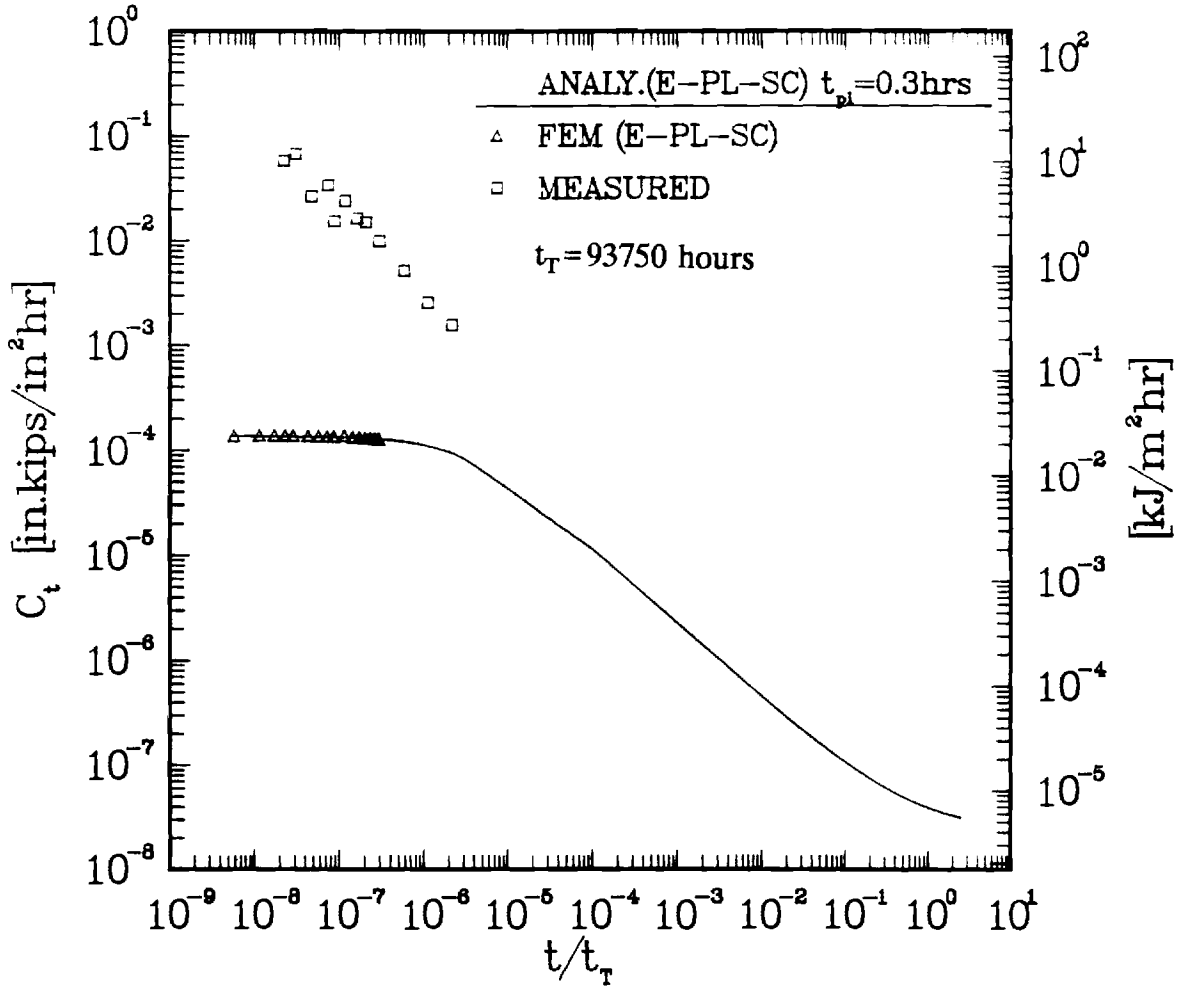

Figure 4: Measured C_t values from the first cycle of a 0.0278 hour hold time test compared with FEM and analytical prediction for an elastic-plastic-secondary creep model.

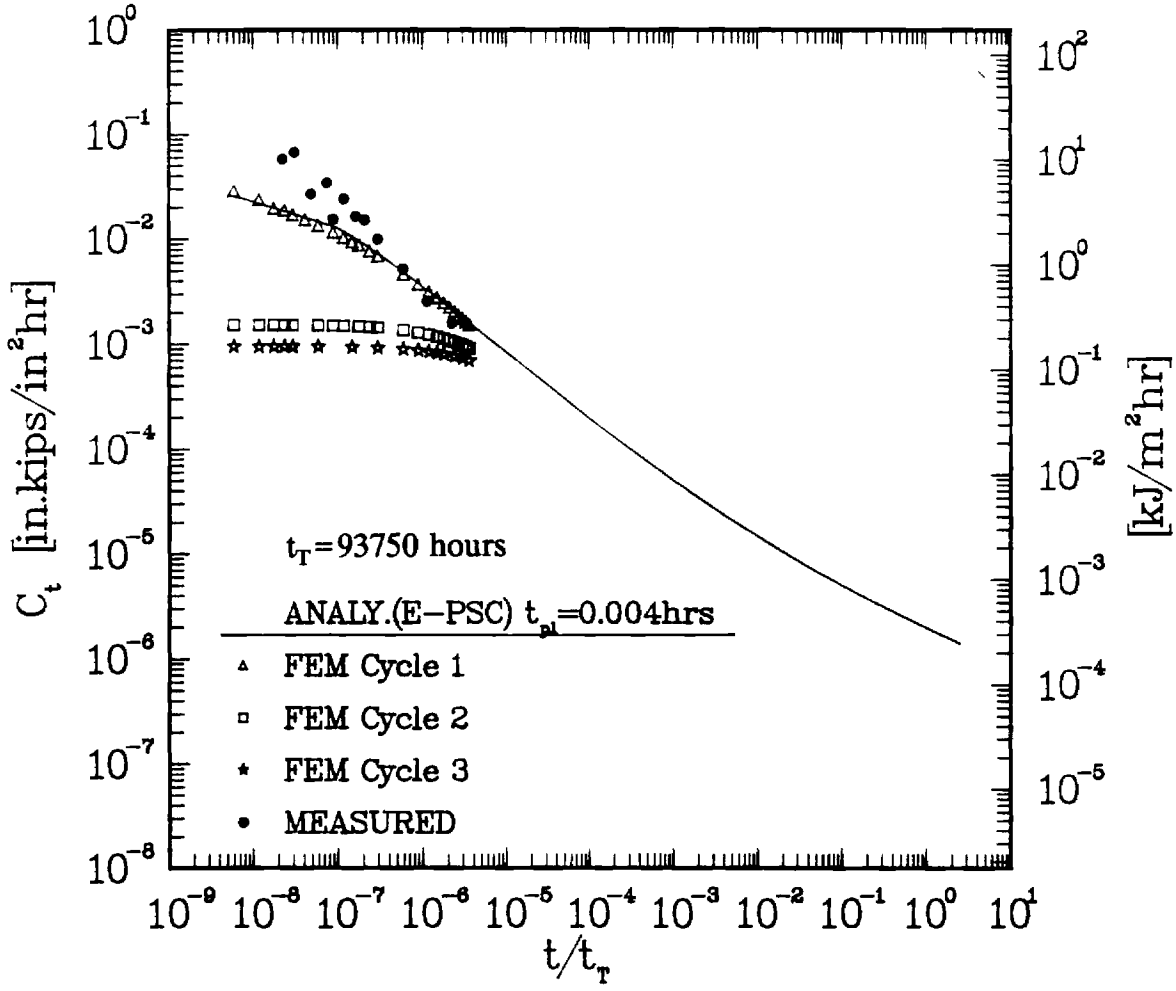

Figure 5a: C_t as a function of normalized time for three cycles from the FEM analyses with 20 minutes hold time including primary creep. The measured C_t values for the first cycle are also included.

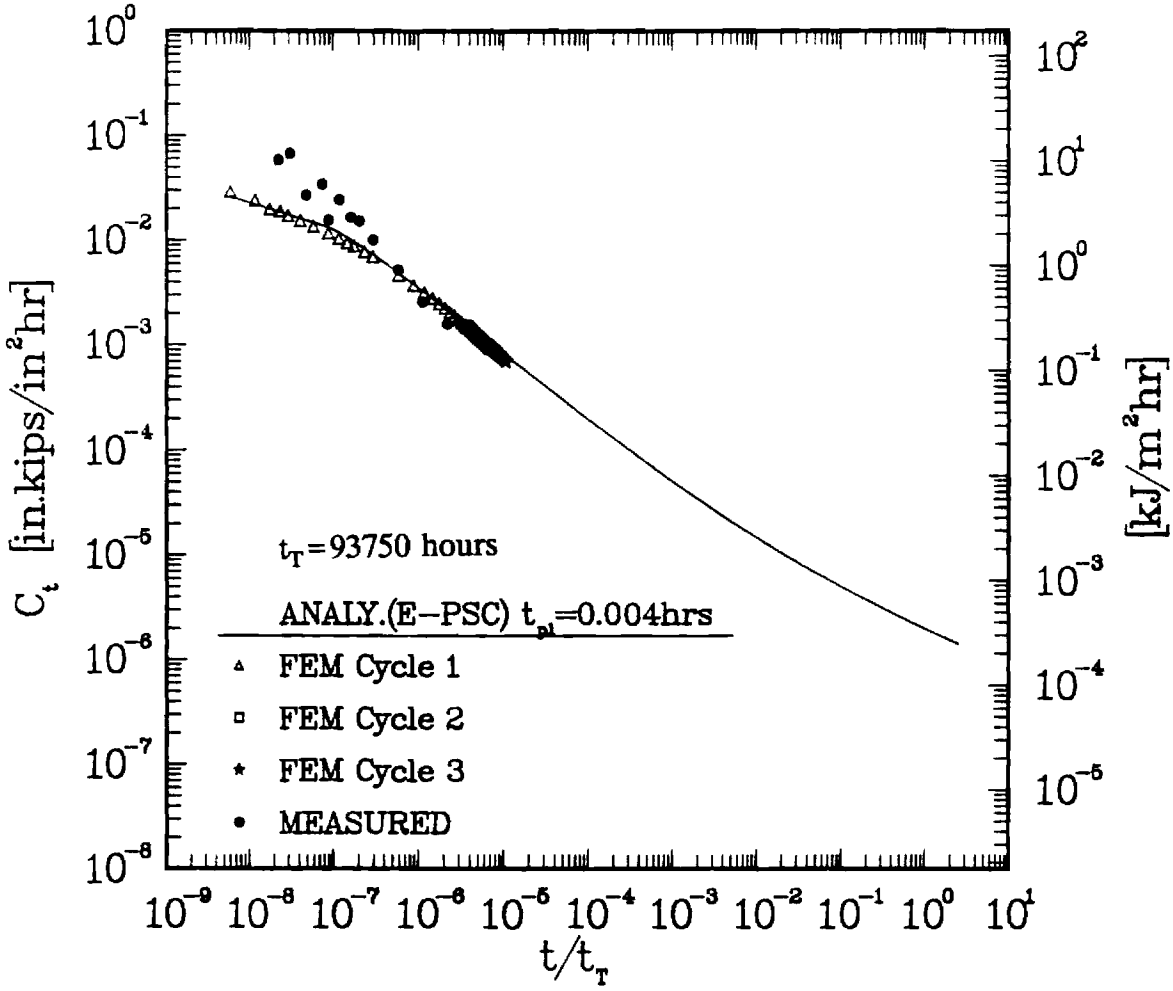

Figure 5b: The same data as in Fig. 5a, except, the time for the second and the third cycles is taken cumulatively instead of referencing it to the start of the hold period during each cycle.

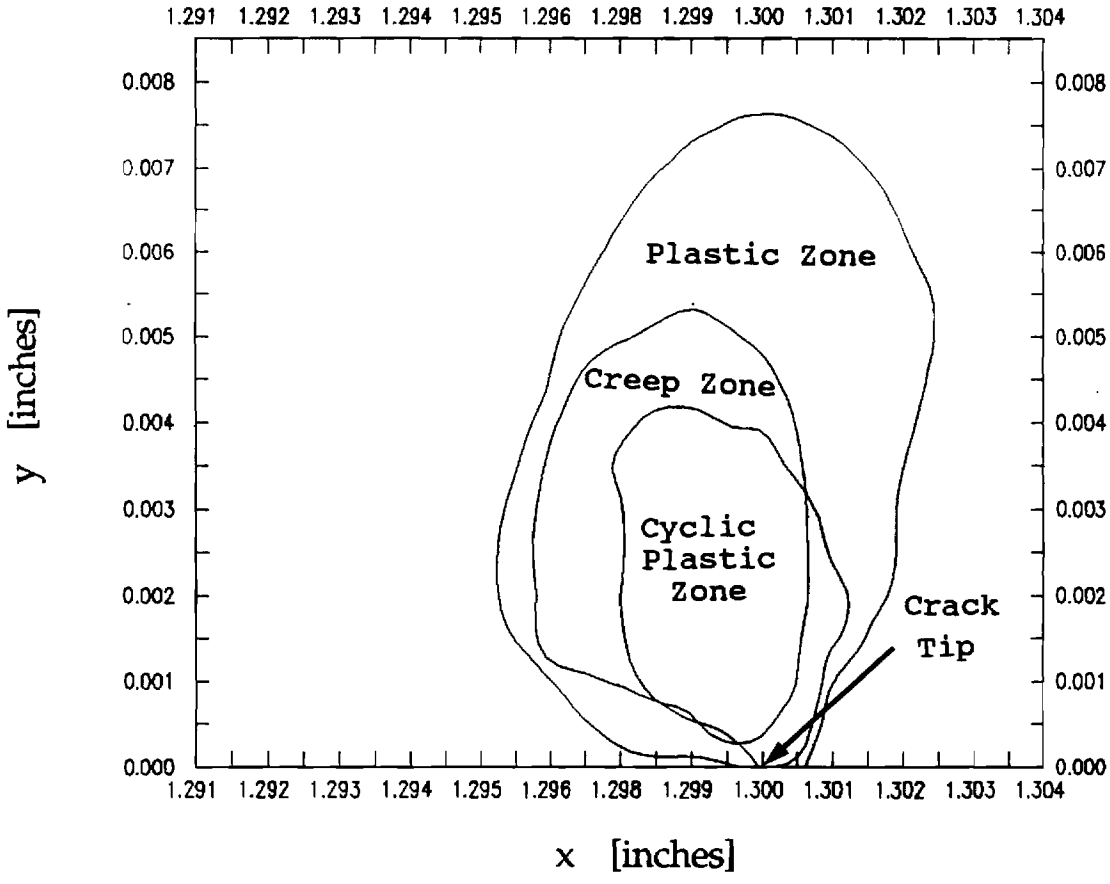

Figure 6: Relative sizes of the cyclic and monotonic plastic and creep zones at the end of the third cycle.

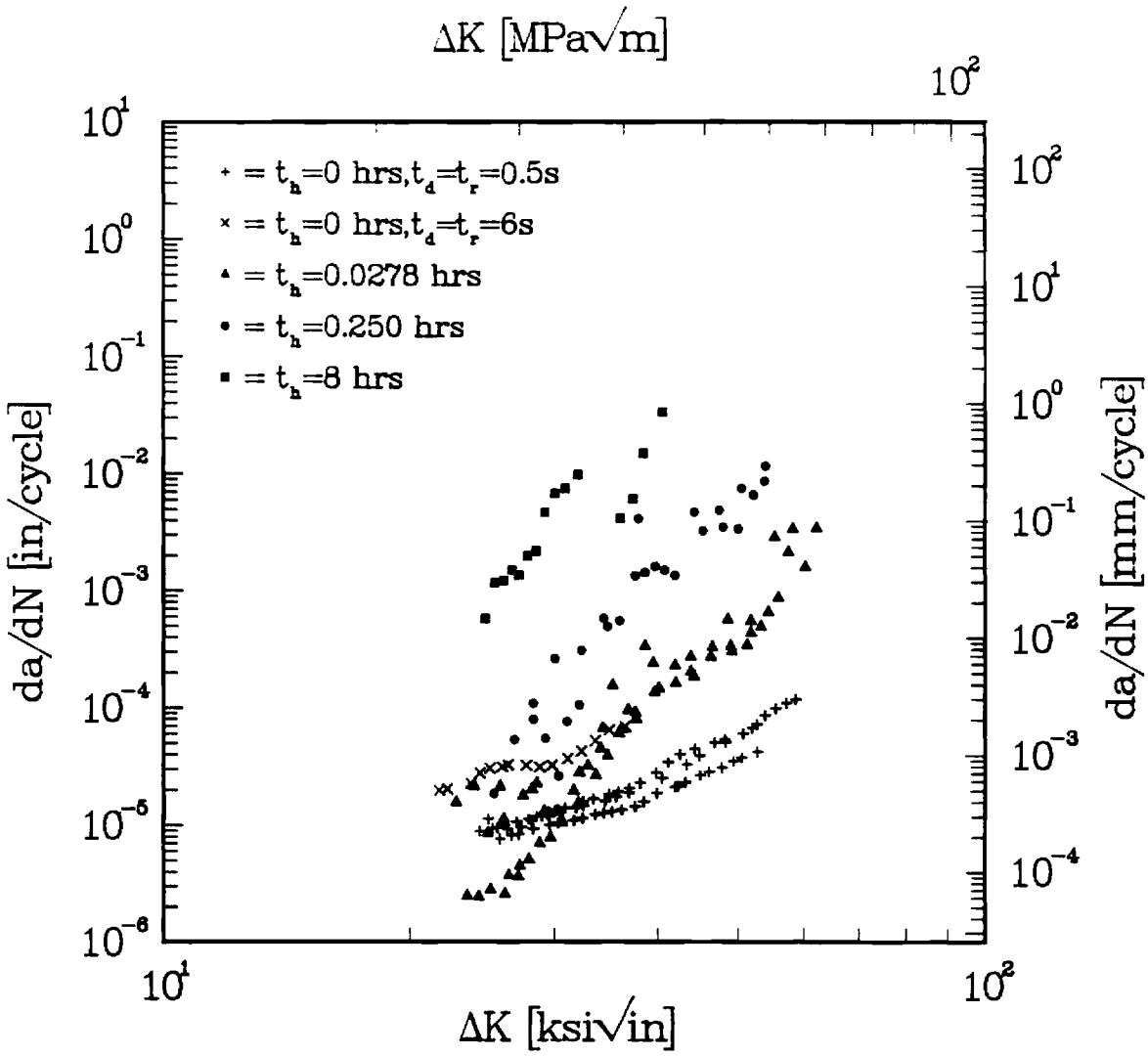

Figure 7: Cyclic crack growth rate, da/dN, as a function the stress intensity factor, ΔK, for different hold times.

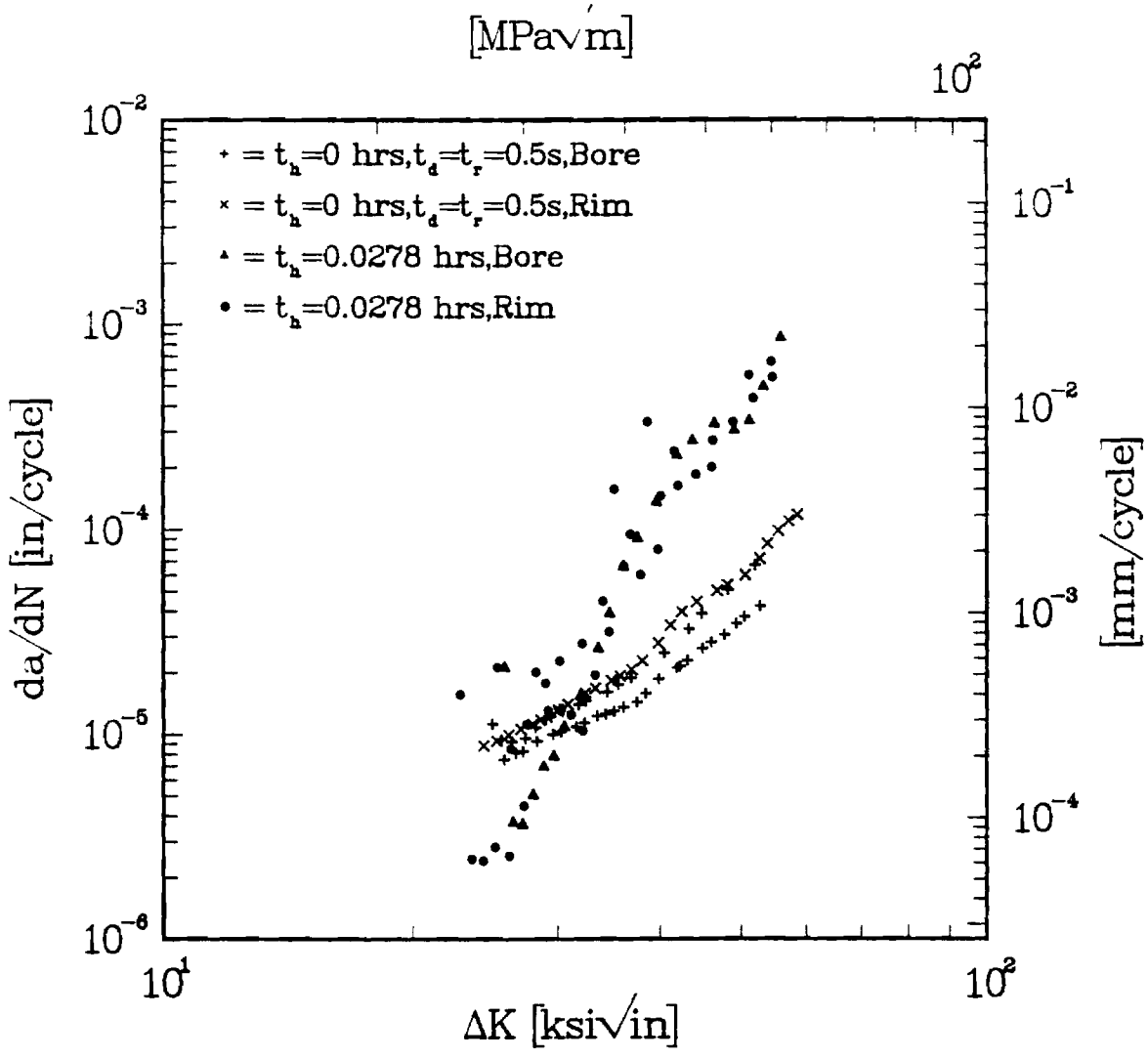

Figure 8: The influence of specimen location (Bore and Rim) on the cyclic crack growth rate.

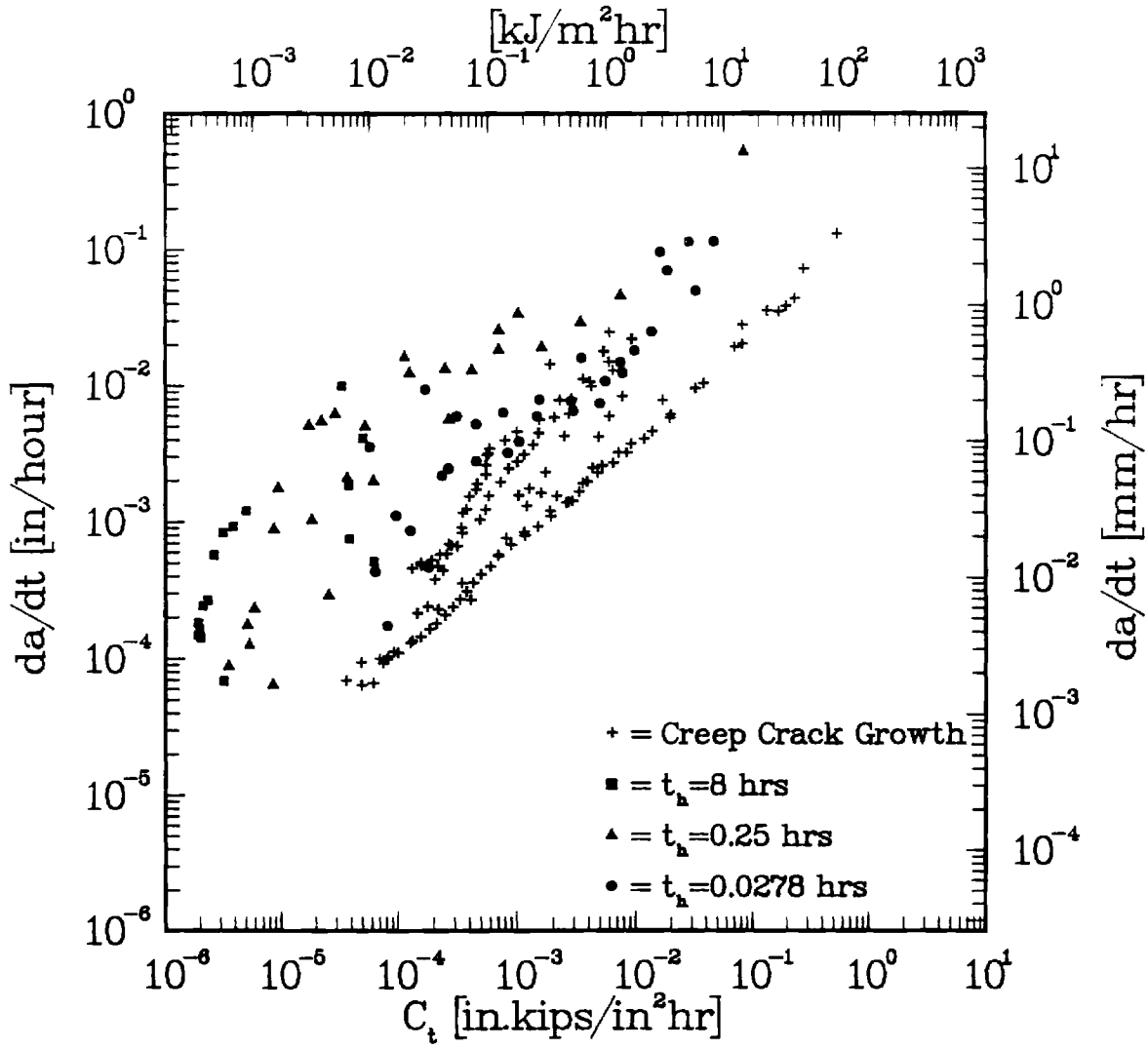

Figure 9: Representation of the creep-fatigue crack growth rate data as a function of $(C_t)_{avg}$ for various hold times. The $(C_t)_{avg}$ in this plot is estimated using only the elastic-secondary creep deformation model (i.e. primary creep is not included).

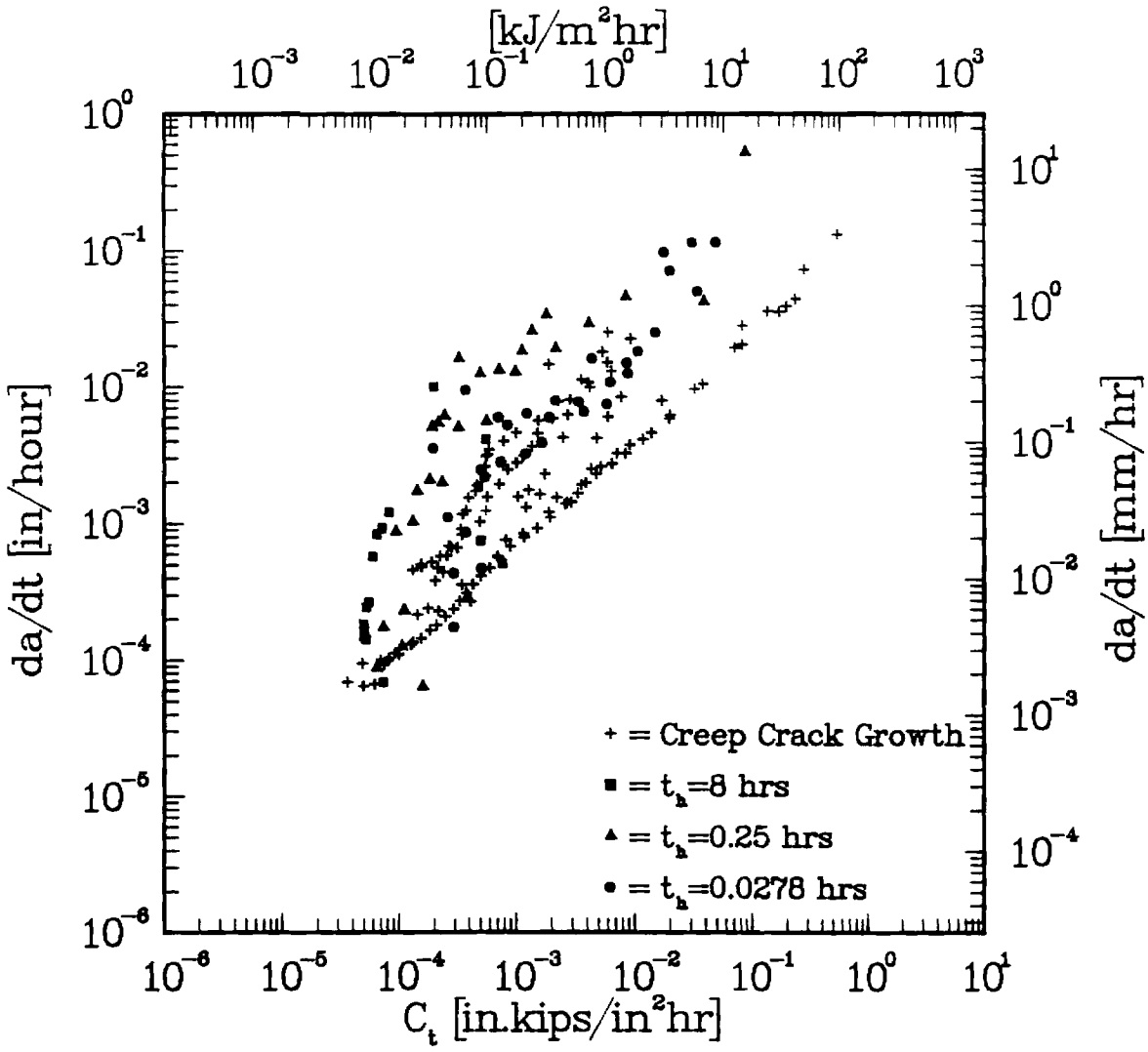

Figure 10: The same data as in Fig. 9 after inclusion of primary creep.

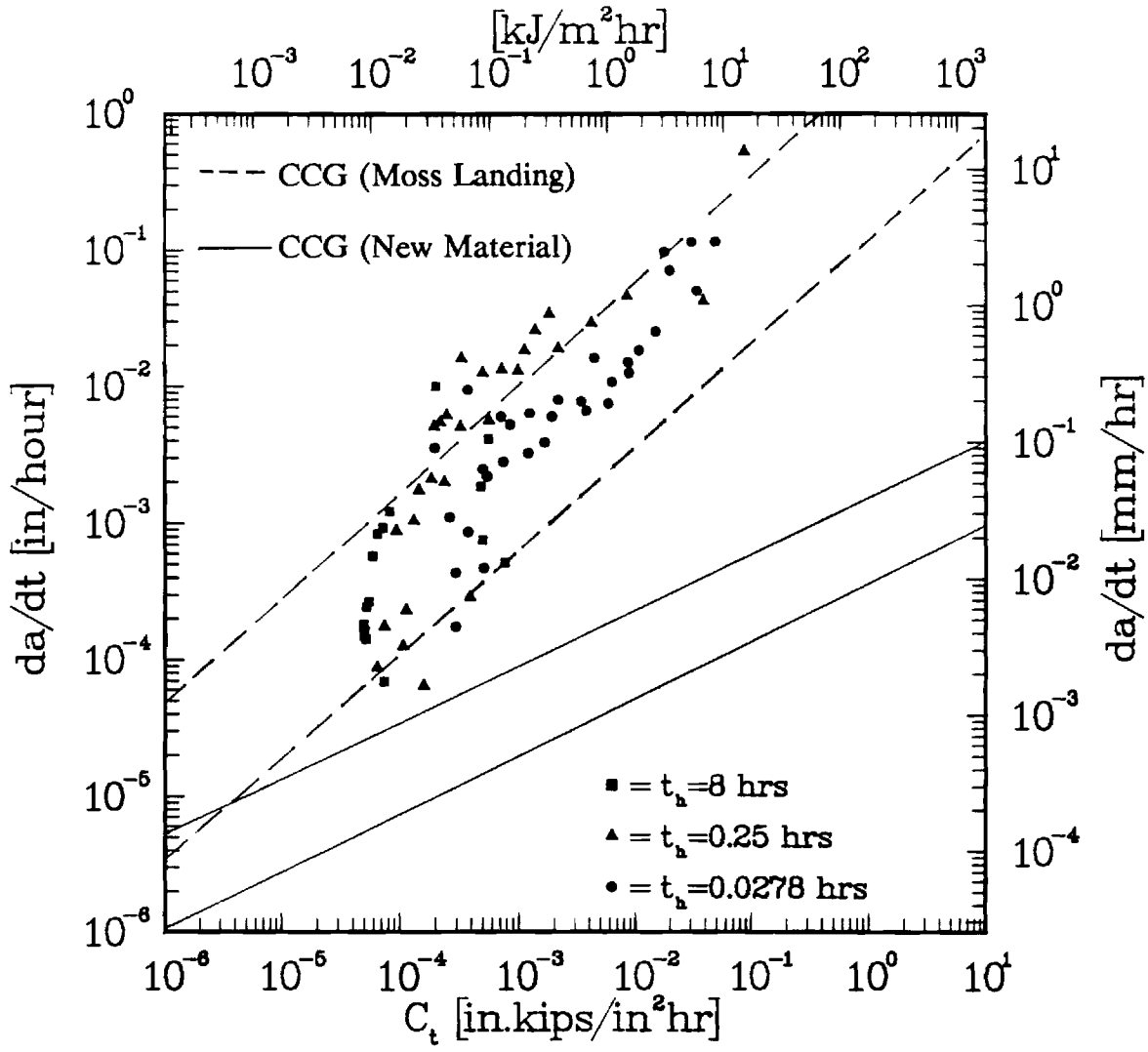

Figure 11: Comparison of ex-service creep-fatigue crack growth rate data with CCG rate from New Material.

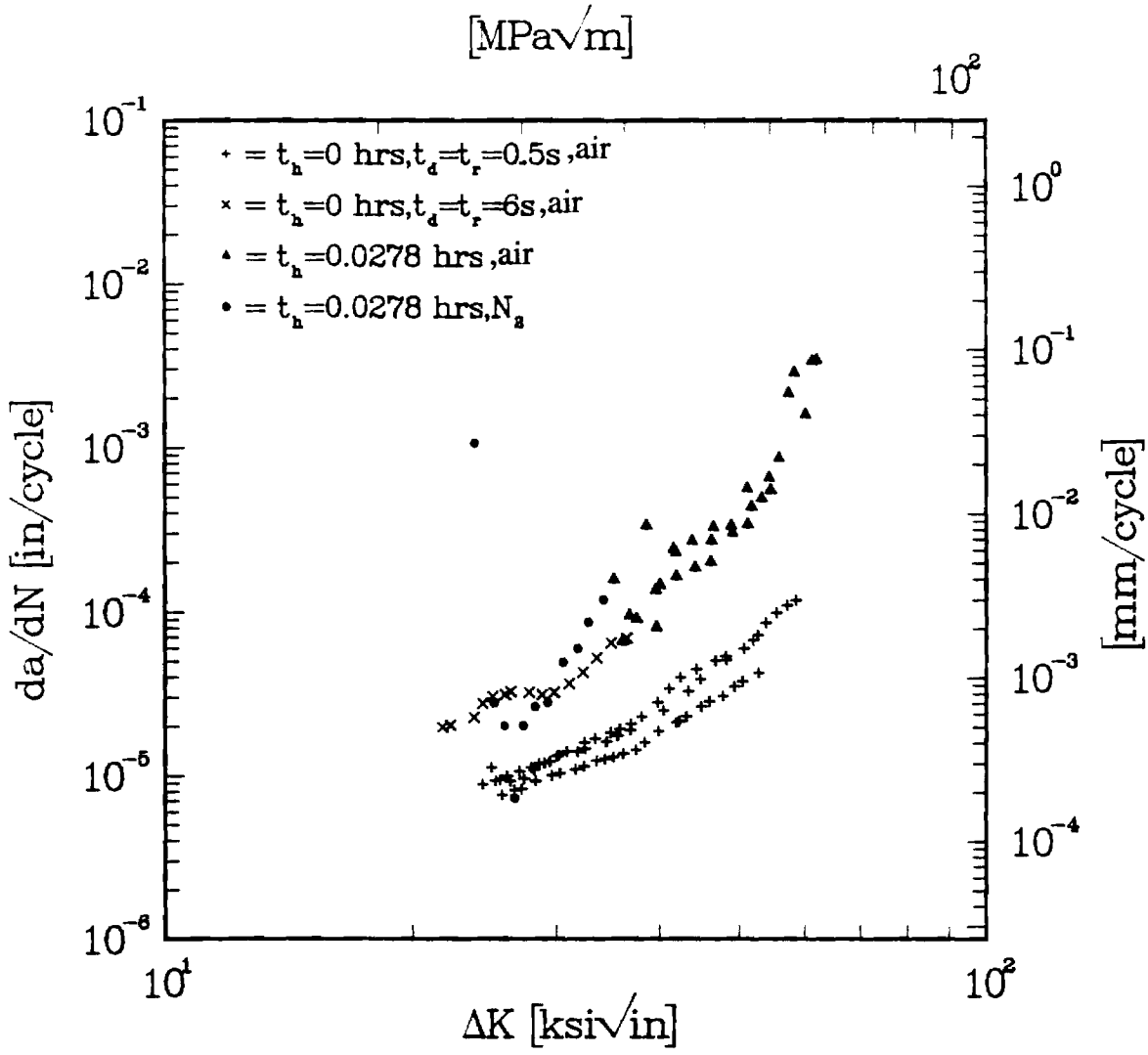

Figure 12: CFCG tests in high purity Nitrogen environment correlations of da/dN versus ΔK.

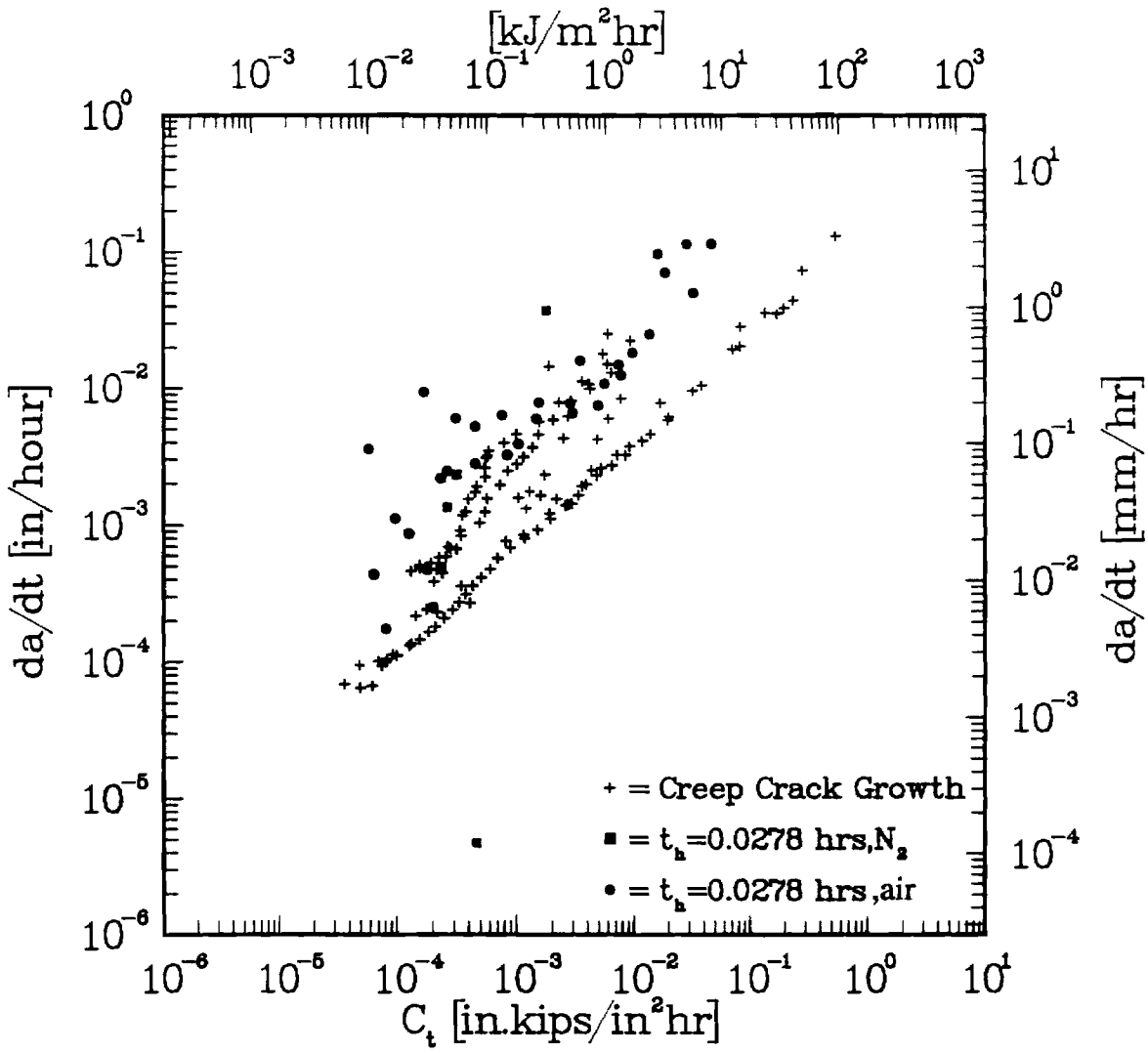

Figure 13: CFCG tests in high purity Nitrogen environment correlation of da/dt versus $(C_t)_{avg}$.